THE JOURNAL OF PHYSICAL CHEMISTRY B

Article

pubs.acs.org/JPCB

# Budding Pathway in the Templated Assembly of Viruslike Particles

Andrey G. Malyutin and Bogdan Dragnea*

Department of Chemistry, Indiana University, 800 E. Kirkwood Avenue, Bloomington, Indiana 47405, United States

Supporting Information

**ABSTRACT:** A new pathway for the assembly of viral capsid protein around inorganic nanoparticle cores was observed by time-course light scattering and cryo-electron tomography. Gold nanoparticles with an average diameter of 11.3 nm have been used as a template for the assembly of Brome mosaic virus (BMV) capsid protein at different concentrations. At least at low protein concentrations the kinetic features of the scattering and extinction measurements are consistent with the initial rapid formation of large nanoparticle−protein clusters, which subsequently separate into individual viruslike particles (VLPs). The occurrence of multiparticle clusters at short times after mixing nanoparticles and proteins was confirmed by cryo-EM. Cryo-electron tomography of the multiparticle clusters yielded an average surface-to-surface interparticle distance of ∼7.5 nm, equivalent to ∼1.5 times the thickness of a protein shell. We propose a scenario in which VLP generation may take place through monomer exchange between aggregated particles with defect-ridden or incomplete shells, leading to the formation of stable icosahedral shells, which eventually bud off the aggregate. Together with results from previous works, the findings highlight the astonishing versatility of plant virus capsid protein assembly. This previously unknown mechanism for VLP formation has features that may have relevance for the crowded environment characterizing virus factories in the cell.

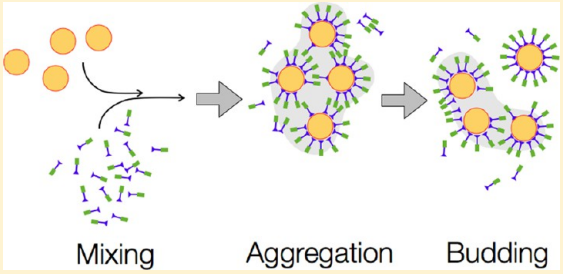


## 1. INTRODUCTION

Regularity in the shape and size of small plant viruses has long been[1] a source of vivid interest across the physical[2,3] and life sciences[4] not only because of the astonishing stoichiometric precision with which hundreds of molecular building blocks fit into the final structure but also because it occurs without external intervention, by a spontaneous and efficient self-assembly process.[5] Attaining similar efficiency and precision in man-made self-assembling systems at spatial scales from several nanometers to micrometers remains an elusive goal.[6] Very early on in the study of virus assembly, it was recognized that, along with subunit selectivity, the nature of available assembly pathways is likely to play a crucial role.[7]

However, details of assembly mechanisms are not available for any virus. Assembly reaction kinetics have been discussed according to the homogeneous or heterogeneous nature of the nucleation step.[8] At least for some plant viruses, the coat protein can assemble by both nucleation mechanisms, albeit under different conditions. Here we show that the versatility of the BMV coat protein exceeds these limits, and we describe a previously unobserved mechanism of assembly involving reversible aggregation as an intermediate step.

BMV is a small plant virus with a capsid composed of 180 copies of the 20 kDa coat protein and a tripartite single-stranded RNA genome.[9] The structure of the BMV capsid protein obeys the canonical jellyroll motif encountered in many simple icosahedral viruses.[10] This typical organization involves an arginine-rich, positively charged, flexible domain interacting electrostatically with the nucleic acid inside the capsid and an outer domain, of well-defined structure, responsible for icosahedral organization by extended contact interactions between coat proteins.[11] The canonical structural organization and the fact that the capsid can be readily disassembled and reassembled in vitro established BMV as an early model system for icosahedral ssRNA virus assembly.[12] As such, much work has been done to understand the pathways of assembly of BMV and its close relative, the cowpea chlorotic mottle virus (CCMV), into empty capsids[13] and around genomic[14] or abiotic cargo cores.[15] Primarily on the basis of in vitro experimental observations,[16] two main scenarios emerged aiming at describing the assembly around the polyanionic cargo.[8b,17] The first involves two distinct steps: (1) loose initial association of a large number of CPs and cargo and (2) annealing of the disordered loosely bound complex into a final capsid structure caging the cargo. The second scenario, reminiscent of an assembly line, involves the nucleated growth of the icosahedron by the sequential addition of subunits. In both cases, the polyanion serves as a heterogeneous nucleus lowering the activation energy barrier to protein−protein association. Hagan and colleagues have shown that, in computational assembly models, varying cargo−subunit and subunit−subunit relative interaction strengths may lead to switching between the two scenarios.[8e,f]

Although most experimental studies aiming at elucidating the mechanisms of self-assembly from kinetic data concentrated on empty capsids, few have examined the assembly kinetics in the

**Received:** June 6, 2013
**Revised:** August 13, 2013

   dx.doi.org/10.1021/jp405603m | J. Phys. Chem. B XXXX, XXX, XXX−XXX

presence of polyanionic cargo.[16a] This is because the kinetics of assembly is very rapid in the presence of polyanions, being driven by long-range strong electrostatic interactions.[8e,f,h] Methods that operate under physiological conditions on unlabeled samples, such as small-angle neutron scattering (SANS), can discriminate between nucleic acid and protein but lack sufficient time resolution, being able to capture only initial and final states of disassembly and assembly.[16a] Recent time-resolved small-angle X-ray scattering (SAXS) work on the simian virus 40 CP assembly of around 500mer RNA provided support for the cooperative rapid binding of subunits to an initial nucleoprotein complex without further annealing.[8h]

However, because SAXS suffers from an absence of protein/nucleic acid contrast, it is difficult to follow the separate fates of the CP and the nucleic acid. The templated assembly of viruslike particles provides an alternative method of measuring assembly kinetics in the presence of polyanionic cargo by light scattering while benefiting from differential cargo/protein contrast (by electron microscopy) and large scattering cross sections and hence time resolution.[18] In this method, polyanionic gold nanoparticles (Au NPs) of diameter commensurate with that of the inner virus coat cavity replace the nucleic acid in the final assembly. With proper Au NP functionalization and choice of buffers, assembly results in viruslike particles with protein cages that are structurally similar to those of wild-type viruses and their mutants.[19]

In this work, we examined the light-scattering intensity and light extinction versus time during the assembly process of BMV VLPs after mixing capsid proteins in different concentrations with a fixed number of polyanionic nanoparticles. Cryo-electron tomography[20] was performed on frozen samples at different stages of the assembly process to obtain structural organization information according the constrained interpretation of scattering data.

## 2. METHODS

**2.1. Time-Course Light-Scattering Intensity.** Scattering and extinction signals were collected as a function of time using a 405 nm laser source in a homemade setup consisting of a three-way temperature-controlled quartz cuvette, an avalanche photodiode detector for scattered light, and a Si pin detector for transmitted light measurements. A 0.1 numerical aperture lens having its optical axis at 90° with respect to the laser was used to collect a fraction of the scattered light. Low-noise preamplified signals were recorded by a two-channel digital oscilloscope at a 1 ms time step. Because extinction is dominated by NP absorption, the extinction signal served as a control for the total number of Au NPs present in the beam (thus avoiding possible precipitation artifacts).

Solutions of 30.8 nM NP were prepared at pH 4.5 and an ionic strength of 0.15 M. Free CP monomers (40 $\mu$L) at concentrations of between 0.6 and 24.5 $\mu$M at pH 7.5, $I_s \approx 0.07$ M, were mixed with Au NP solutions (mixing time ~1 s). Specifically, samples were prepared in two parts, solutions A and B. Solution A was a mixture of 50 $\mu$L of SAMA buffer [50 mM NaOAc, 8 mM $Mg(OAc)_2$ (pH 4.5)] in a small volume, usually no more than 4 $\mu$L, of highly concentrated NP solution. This portion was further adjusted to 60 $\mu$L typically with TKM buffer [1 M KCl, 10 mM Tris, 5 mM $MgCl_2$ (pH≈≈ 7.4)] and MQ water to ensure a final ionic strength of about 0.15 M. Solution B was 40 $\mu$L of CP in TNKM buffer [50 mM tris, 50 mM NaCl, 10 mM KCl, 5 mM $Mg_2Cl$ (pH 7.4)]. For 90:1 dimers to NP experiments, solution B was 15.3 $\mu$M, for a final monomer concentration of 6.1 $\mu$M once combined with solution A.

In a typical experiment, solution A was pipetted into the three-way cuvette and allowed to equilibrate at the set temperature for 10 min. Solution B is then introduced and mixed with a pipet. A stopper was designed to position the tip reproducibly for mixing. Scattering and extinction signals were collected for 100 to 2000 s.

A limited data set from a stopped-flow instrument (SF-300X Kintek) providing faster mixing times was also acquired. All measurements were conducted at 20 °C and at 405 nm wavelength. A 20 $\mu$L injection of 61.6 nM gold NPs in SAMA buffer (with $I \approx 0.2$ M) was mixed with a 20 $\mu$L injection of 12.3 $\mu$M CP in TNKM buffer. Three traces were collected per experiment, with a dead time after mixing of ~0.01 s.

**2.2. Au NP Preparation.** Citrate-coated gold nanoparticles were prepared according to the Slot and Geuze method[21] and subsequently functionalized with a HS-$C_{11}$-TEG-$CH_2CO_2H$ ligand as described previously.[22]

**2.3. Virus Preparation and Protein Purification.** BMV was expressed in *Nicotiana benthamiana* via *Agrobacterium*-mediated gene delivery. Seven days postinfection, the leaves were collected and homogenized in virus buffer [250 mM NaOAc, 10 mM $MgCl_2$ (pH 4.5)] and then centrifuged at 5000 rpm for 25 min on a Beckman TA-10.250 rotor. The supernatant was then layered on a 10% sucrose cushion (virus buffer) and centrifuged at 26 000 rpm for 3 h on a Beckman SW 32 rotor. The pellets were resuspended in 38.5% CsCl (w/v, virus buffer) and banded by centrifugation at 45 000 rpm for 24 h on a Beckman TI-71 rotor. The translucent virion band was collected and dialyzed, with three changes, against SAMA buffer. Final purity was achieved by running the virus on a Superose-6 column by FPLC. The purified virus was dialyzed against disassembly buffer [500 mM $CaCl_2$ (pH 7.4)] with three changes to precipitate RNA. Solution was centrifuged for 30 min at 35 000 rm using a Beckman TLA110 rotor. The supernatant was dialyzed against Tris [10 mM Tris (pH 7.4)] and then TNKM. Protein dimers were stored at 4 °C for the duration of the experiments.

**2.4. Cryo-Electron Tomography.** A 2.4 $\mu$L drop of solution A was applied to C-Flat grids (1.2 $\mu$m holes, 1.1 $\mu$m spacing, 200 mesh) that were freshly glow discharged for 40 s. Solution B (1.6 $\mu$L) was rapidly mixed with NP solution A on the grid. Grids were then immediately blotted manually from the back and plunge frozen under ambient conditions. Images and tomograms were collected on a JEOL JEM 3200FS FEG TEM, at a 300 kV accelerating voltage, equipped with an energy filter and a Gatan UltraScan 4000 CCD camera. Serial EM was used to collect tomograms, and etomo was utilized for reconstruction.[23]

## 3. RESULTS AND DISCUSSION

Figure 1 shows a comparison between empty capsid and VLP growth kinetics at initial CP concentrations of 24.5 and 6 $\mu$M, respectively. Empty capsid kinetics (Figure 1a) is much slower than VLP kinetics (Figure 1b), which is practically instantaneous with respect to mixing. The assembly of VLPs and capsids was confirmed by negative stain transmission electron microscopy of samples collected at long times after mixing. The initial scattering intensity level in Figure 1b is dominated by scattering from Au NPs. After equilibration, the scattered light intensity level is ~3.5 times higher than the initial value (from bare Au NPs). This is due to an increase in particle polarizability from the adsorption of protein on the Au NP surface. For a homogeneous sphere,[24]

$$\alpha = 4\pi \in_0 a^3 \frac{\in_1 - \in_m}{\in_1 + 2\in_m} \tag{1}$$

where $\alpha$ is the polarizability, $a$ is the particle radius, $\varepsilon_1$ is the relative permittivity of the sphere material, and $\varepsilon_m$ is the relative permittivity of the medium. For a coated sphere,[24]

$$\alpha = 4\pi \in_0 a_2^3 \times \frac{(\in_2 - \in_m)(\in_1 + 2\in_2) + f(\in_1 - \in_2)(\in_m + 2\in_2)}{(\in_2 + 2\in_m)(\in_1 + 2\in_2) + f(2\in_2 - 2\in_m)(\in_1 - \in_2)} \tag{2}$$


dx.doi.org/10.1021/jp405603m | J. Phys. Chem. B XXXX, XXX, XXX−XXX

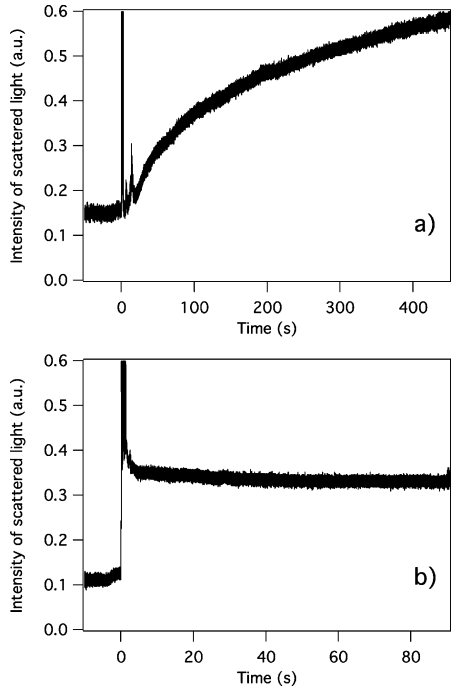


**Figure 1.** Time-course light-scattering intensity for (a) empty capsid kinetics and (b) VLP assembly at a CP/NP dimer to NP ratio of 360:1. Note the large initial increase in the scattering intensity followed by signal decay to a value above that of Au NPs alone.

where $\alpha$ is the polarizability, $a_1$ is the core particle radius, $a_2$ is the outer particle radius, $\varepsilon_1$ is the permittivity of the core sphere material (complex for Au), $\varepsilon_2$ is the permittivity of the shell material (protein), $\varepsilon_m$ is the permittivity of the medium (water), and $f$ is the fraction of the total spherical volume occupied by the core.

A graphic comparison of polarizabilities for a bare particle and a protein-coated particle is presented in Figure 2. The following numerical values have been used: $a_1$ = 6 nm, $a_2$ = 14 nm, $\varepsilon_1$ versus energy data for gold taken from Olson et al.,[25] $\varepsilon_2$ = 3,[26] and $\varepsilon_m$ = 1.77. At 405 nm (~3 eV), the particle polarizability increases ~4-fold upon coating with a protein monolayer. Because the scattering cross section is proportional to the square of optical polarizability,[24] the association of the

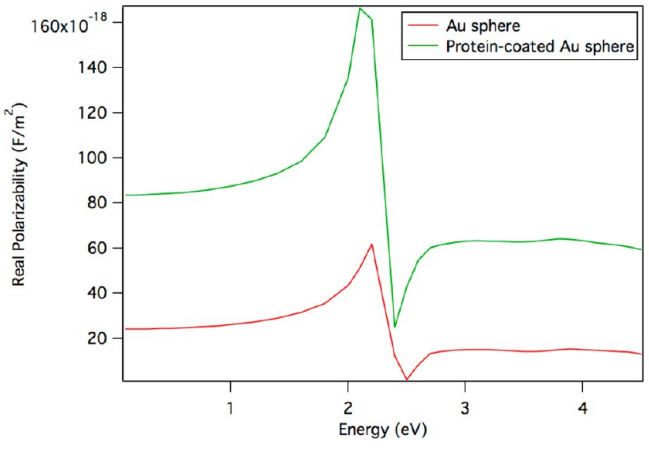


**Figure 2.** Coating of a gold sphere by a monolayer of protein increases the particle polarizability several times (graphs corresponding to eqs 1 and 2).

coat protein -(CP) with the particle core is easily detectable as an increase in the scattering signal relative to bare particles, which is observed at late times in Figure 1. Indeed, transmission electron microscopy confirmed that after equilibration more than 80% of the Au NPs were coated with a complete CP layer. Two other points regarding Figure 1 are worth noting: First, there is a sharp increase in the scattering signal immediately after mixing, followed by fast decay (~2 s) to the equilibrium value that, as we have seen, corresponds to the complete coating of Au NPs by CP. This must be a different state than that of dispersed individual VLPs that we have found by TEM at long times after equilibration. The question is what state of the sample is responsible for this rise, which is absent in empty capsid assembly kinetics (Figure 1 a)? Second, under the conditions of Figure 1, assembly is at least 2 orders of magnitude faster for NP-filled capsids than for empty capsids. Mixing uncharged particles with CP does not exhibit any of the above features.

To investigate the mechanisms responsible for the qualitative difference, we studied how VLP assembly kinetic rates depend on CP concentration. Figure 3 shows light-scattering kinetic

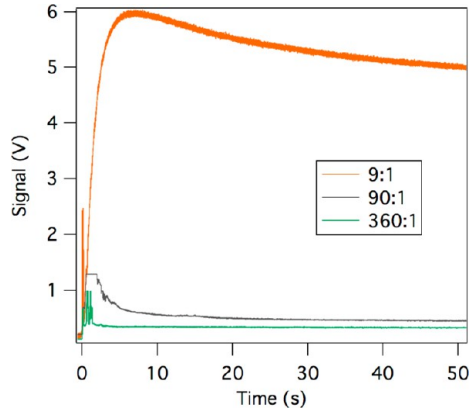


**Figure 3.** Time-course scattering curves for mixtures of BMV capsid protein and Au nanoparticles at different molar fractions.

traces for three ratios of CP to Au NP: 360:1, 90:1, and 9:1. The Au NP concentration was kept constant at 30.8 nM. Again, an early increase in the signal followed by a decay to the steady-state-enhanced scattering level can be recognized in all traces. However, at substoichiometric CP/NP ratios (e.g., 9:1) the increase is slower and the signal tends to stabilize after decay to a higher value than the value associated with completely coated NPs. In other words, the more dilute the CP solution, the higher the initial scattering intensity and the slower the subsequent decay. Because absorbance remained essentially unchanged after mixing (Figure S1, Supporting Information), the decay following the initial increase must be associated with a process that maintains the same number of absorbing particles in the beam (i.e., the hypothesis of potential artifacts due to the precipitation of material out of the probe beam can be excluded). Because the scattering intensity is very sensitive to changes in the radial correlation function at small distances between particles,[27] we hypothesized that this might be due to the initial aggregation of multiple NPs facilitated by CP/NP electrostatic interactions, followed by the break up of multiparticle aggregate. It can be shown for particular examples that such aggregates have scattering cross sections that are larger than the sum of the cross sections of individual particles


dx.doi.org/10.1021/jp405603m | J. Phys. Chem. B XXXX, XXX, XXX−XXX

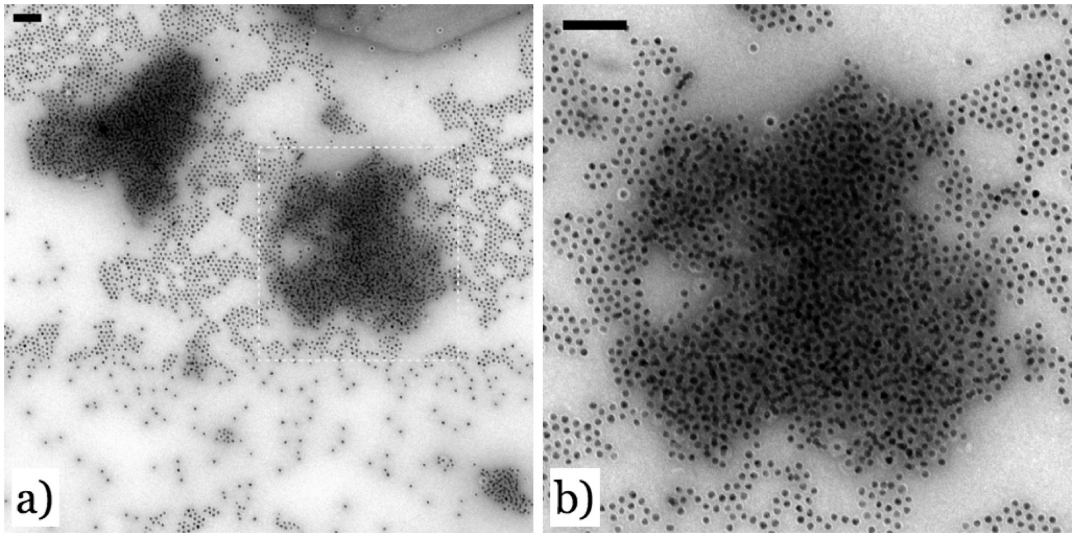


**Figure 4.** (a) Negative stain TEM of a 90:1 CP dimer to NP ratio sample, 6 s after mixing. Scale bar = 100 nm. (b) Close-up view of the area enclosed by the dotted square in a. At the periphery of the dark cluster in b, one can notice several nearly complete VLPs.

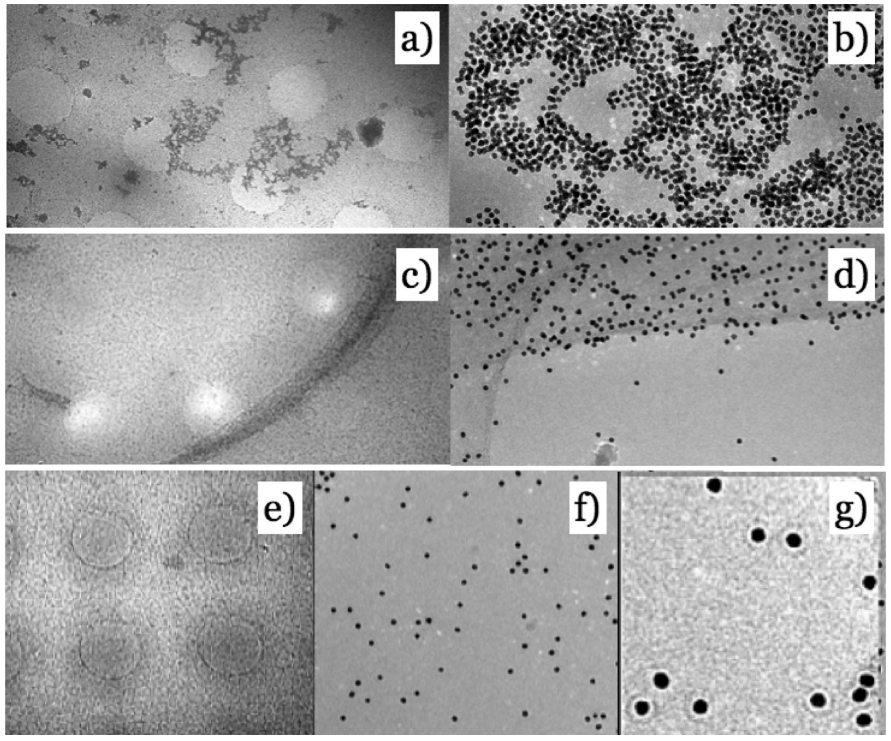


**Figure 5.** Cryo-EM images at (a) low magnification and (b) high magnification for a sample frozen ~6 s after mixing (assembly start). Twenty seconds after assembly at (c) low magnification and (d) higher magnification. Two hours after assembly started, no clusters could be observed at (e) low magnification and (f) high magnification and (g) for a close-up view of the area in panel f showing complete CP shells surrounding individual Au NPs.

making the aggregate.[24] In addition, multiple scattering events further increase the scattering intensity from dense aggregates when compared to that of sparse aggregates. Note that, for the concentration range studied here, depletion forces seem to have a negligible effect with respect to electrostatic interactions as shown by the lack of association interactions in the absence of NP surface charge. Moreover, the initial jump in scattering intensity is inversely proportional to the concentration whereas a deplection effect would be expected to be directly proportional to it.

To test directly for the existence of clusters of NPs, samples were prepared directly on carbon-coated TEM grids and imaged by negative-stain TEM (Figure 4). Large clusters of NPs and presumably CP as well as dispersed complete VLPs, incomplete VLPs, nearly complete VLPs, and VLPs budding out an aggregate could be seen.

Furthermore, to circumvent the possibility of artifacts that could be caused by NP/grid surface interactions, drying, and staining, similar samples were prepared and frozen at different times after the beginning of the reaction for observations by cryo-EM.


dx.doi.org/10.1021/jp405603m | J. Phys. Chem. B XXXX, XXX, XXX−XXX

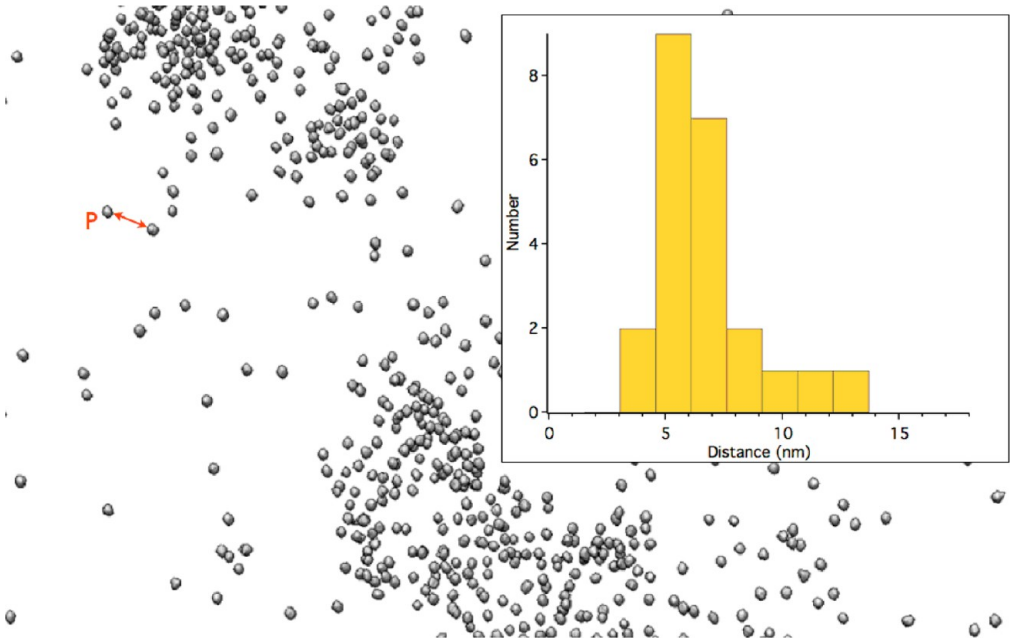


**Figure 6.** Tomographic 3D reconstruction showing clusters of Au NPs stabilized by viral CPs. The red arrow represents the surface-to-surface closest-neighbor distance for particle P. Inset: Histogram of closest-neighbor distances.

Figure 5 provides a comparison of typical cryo-EM micrographs of 90:1 CP dimer/Au NP samples frozen in vitreous ice as a function of time after mixing. At short times (~6 s), a variety of loose NP clusters ranging in size to up to several micrometers are readily noticeable. Only the largest clusters survive past 20 s into the assembly, with the sample being formed mostly of individual particles. Finally, very few small clusters were observed in VLP samples that were allowed to react for 2 h. Control experiments with nanoparticle solutions without proteins added showed no signs of clustering at any time. Therefore, CP induces clustering immediately after mixing.

Clusters were further analyzed by cryo-electron tomography to determine the average closest-neighbor distance for the Au NPs within a cluster (Figure 6). After the reconstruction of the tilt series, 3-D volumes were used to measure the distance between the surfaces of nearest-neighbor particles. The histogram of surface-to-surface distance reveals a peak at 5.5 nm, with an average separation of 7.5 nm for the entire histogram (Figure 6b). Because the thickness of the BMV capsid is ~5 nm, the average interparticle separation is ~1.5 times the thickness of the protein shell whereas the most probable separation is at one protein shell thickness. This result suggests that each NP carries a partial protein coat. It is not clear, however, whether clusters of particles are encapsulated in an extended CP envelope or if there is a degree of interpenetration of CPs on different particles via hydrophobic interaction despite an entropic cost. In either case, weak-enough association of neighboring particles to allow for rearrangements and the exchange of CPs between NPs seems to occur.

Thus, in contrast to previously studied mechanisms of BMV capsid assembly, at low relative protein concentrations we observe the rapid cluster formation of NP cores and protein dimers followed by the separation of VLPs. Carrying out the same experiments with the native viral cargo, RNA, would have been difficult to interpret because of the challenges related to differentiating between RNA and protein in a TEM image.

An important question born out of these results is whether the same mechanism may operate when CP assembles around native RNA as well. Unfortunately, as mentioned, experimental data is scarce because of the short time scale for the process. A notable exception is the recent kinetic study of RNA encapsulation by SV40-derived capsomers (pentamers) by time-resolved small-angle X-ray scattering, which showed evidence of a two-state mechanism by which the assembly process nucleates at the RNA and continues through a cascade of capsomer addition reactions in which one pentamer is added at a time (the assembly line model).[8h] However, numerical simulations of polymer encapsulation suggested that the association of CP with a longer polymer may result in multiple nuclei that are unable to anneal and encapsulate the polymer simultaneously and instead yield disordered aggregates.[8f] Subsequent CP redistribution pathways are required to complete theassembly. Experiments in ref 8h were carried out with short RNA molecules (554 nt; the shortest known viral genomes of ssDNA circoviruses are ~2 kb). However, because assembly pathways depend on the length of the polyanionic cargo it may be possible that the budding mechanism discussed here is pertinent to RNA encapsidation as well.

Another possibility is that the budding mechanism is an exclusive characteristic of VLPs formed on rigid spherical cores. In this case, further study would provide an opportunity for deepening our mechanistic insight, specifically in relation to cargo flexibility. Interestingly, in a recent numerical simulation study of patchy particle assembly on spherical templates, Williamson et al. reported on the observation of a similar pathway that is valid for certain conditions of temperature and interaction anisotropy.[28] Additionally, calculations by Zandi et al. on the assembly of icosahedral capsids around linear and branched chains showed similar behavior for the transition from unassembled to assembled states at various genome to protein ratios.[29]

A final remark concerns whether the initial clustering is a characteristic of substoichiometric CP to Au NP ratios only or if it also actually occurs at high CP molar fractions. We have


dx.doi.org/10.1021/jp405603m | J. Phys. Chem. B XXXX, XXX, XXX−XXX

seen that the lower the CP/Au NP ratio, the slower the initial cluster formation (but the larger the clusters) (Figure 3). Because CP/Au NP ratios greater than 90 result in VLP assembly that is too fast to be followed by our setup, we have utilized a stopped-flow instrument to measure sample transmittance as a function of time. This approach offered the advantage of significantly shorter dead times after mixing (Methods). We have found that even for the above stoichiometric CP/Au NP ratios an initial rapid increase in scattering followed by a decay is present, although the magnitude of the initial increase is only a fraction from that observed at substoichiometric ratios (Supporting Information, Figure S2). This interpretation is supported by kinetic observations of native fluorescence emission that has an initial increase at short times, followed by a decrease at longer times (Supporting Information, Figure S3). This behavior could be attributed to a qualitatively different rearrangement of proteins around NP in the vicinity of NP cores, with most metal-induced quenching occurring in the VLP state and less quenching occurring in the multiparticle state. Therefore, at high CP/Au NP molar ratios clusters form, but they are probably small and short-lived; in this case, the previously established direct VLP formation route is kinetically favored.

## 4. CONCLUSIONS

Kinetic studies of templated BMV VLP assembly combined with cryo-electron tomography suggest the existence of a new possible assembly mechanism in addition to two previously discussed generic icosahedral assembly pathways. The VLP assembly mechanism involves initial rapid cluster formation of NPs and protein dimers. Large clusters are long-lived at very low CP/NP ratios (below ~9:1), but for higher CP concentrations, protein exchange occurs within a multi-NP cluster that leads to budding off of stable VLPs and rapid fragmentation or a decrease in the multiparticle cluster size. The observed behavior probably arises from nonspecific initial NP surface charge neutralization by protein dimers interacting with two or more NPs at a time.

These findings highlight the remarkable selectivity of the BMV coat protein that can rescue assembly even in the crowded environment of a polyanion/protein aggregate. Constraints imposed by such an environment are worth considering because of possible closer similarities with the crowded cytoplasm or viral factory environments than with dilute solutions of proteins and nucleic acids commonly utilized in in vitro studies.[30]

## ■ ASSOCIATED CONTENT

### Supporting Information

Extinction and scattering data from stopped-flow experiments. This material is available free of charge via the Internet at http://pubs.acs.org.

## ■ AUTHOR INFORMATION

### Corresponding Author

*E-mail: dragnea@indiana.edu.

### Notes

The authors declare no competing financial interest.

## ■ ACKNOWLEDGMENTS

We are thankful to Dr. David G. Morgan for assistance with cryo-EM and tomography and to the National Science Foundation (grant no. 0832651) and the Human Frontier Science Program for financial support.

## ■ REFERENCES

(1) (a) Crick, F. H.; Watson, J. D. Structure of Small Viruses. *Nature* **1956**, *177*, 473. (b) Caspar, D. L.; Klug, A. Physical Principles in the Construction of Regular Viruses. *Cold Spring Harbor Symp. Quant. Biol.* **1962**, *27*, 1.

(2) Douglas, T.; Young, M. Host-Guest Encapsulation of Materials by Assembled Virus Protein Cages. *Nature* **1998**, *393*, 152.

(3) Bruinsma, R. F.; Gelbart, W. M.; Reguera, D.; Rudnick, J.; Zandi, R. Viral Self-Assembly as a Thermodynamic Process. *Phys. Rev. Lett.* **2003**, *90*, 248101.

(4) Johnson, J.; Speir, J. Quasi-Equivalent Viruses: A Paradigm for Protein Assemblies. *J. Mol. Biol.* **1997**, *269*, 665.

(5) Fraenkel-Conrat, H.; Williams, R. C. Reconstitution of Active Tobacco Mosaic Virus from Its Inactive Protein and Nucleic Acid Components. *Proc. Natl. Acad. Sci. U.S.A.* **1955**, *41*, 690.

(6) Whitesides, G. M.; Grzybowski, B. Self-Assembly at All Scales. *Science* **2002**, *295*, 2418.

(7) (a) Crane, H. R. Principles and Problems of Biological Growth. *Sci. Mon.* **1950**, *70*, 376. (b) Butler, P. J. Self-Assembly of Tobacco Mosaic Virus: the Role of an Intermediate Aggregate in Generating Both Specificity and Speed. *Philos. Trans. R. Soc. London, Sect. B* **1999**, *354*, 537.

(8) (a) Zlotnick, A. To Build a Virus Capsid. An Equilibrium Model of the Self Assembly of Polyhedral Protein Complexes. *J. Mol. Biol.* **1994**, *241*, 59. (b) McPherson, A. Micelle Formation and Crystallization as Paradigms for Virus Assembly. *BioEssays* **2005**, *27*, 447. (c) van der Schoot, P.; Zandi, R. Kinetic Theory of Virus Capsid Assembly. *Phys. Biol.* **2007**, *4*, 296. (d) Wilber, A. W.; Doye, J. P. K.; Louis, A. A.; Noya, E. G.; Miller, M. A.; Wong, P. Reversible Self-Assembly of Patchy Particles into Monodisperse Icosahedral Clusters. *J. Chem. Phys.* **2007**, *127*, 085106. (e) Hagan, M. F. Controlling Viral Capsid Assembly with Templating. *Phys. Rev. E: Stat., Nonlinear, Soft Matter Phys.* **2008**, *77*, 051904. (f) Elrad, O. M.; Hagan, M. F. Encapsulation of a Polymer by an Icosahedral Virus. *Phys. Biol.* **2010**, *7*, 045003. (g) Johnston, I. G.; Louis, A. A.; Doye, J. P. K. Modelling the Self-Assembly of Virus Capsids. *J. Phys.: Condens. Matter* **2010**, *22*, 104101. (h) Kler, S.; Asor, R.; Li, C.; Ginsburg, A.; Harries, D.; Oppenheim, A.; Zlotnick, A.; Raviv, U. RNA Encapsidation by SV40-Derived Nanoparticles Follows a Rapid Two-State Mechanism. *J. Am. Chem. Soc.* **2012**, *134*, 8823.

(9) Kao, C. C.; Sivakumaran, K. Brome Mosaic Virus, Good for an RNA Virologist's Basic Needs. *Mol. Plant Pathol.* **2000**, *1*, 91.

(10) Casjens, S.; King, J. Virus Assembly. *Annu. Rev. Biochem.* **1975**, *44*, 555.

(11) Casjens, S. *Virus Structure and Assembly*; Jones and Bartlett: Boston, 1985.

(12) Bancroft, J. B.; Hills, G. J.; Markham, R. A Study of Self-Assembly Process in a Small Spherical Virus - Formation of Organized Structures From Protein Subunits in Vitro. *Virology* **1967**, *31*, 354.

(13) Pfeiffer, P.; Hirth, L. Aggregation States of Brome Mosaic Virus Protein. *Virology* **1974**, *61*, 160.

(14) (a) Wagner, G. W.; Bancroft, J. B. Self-Assembly of Spherical Viruses with Mixed Coat Proteins. *Virology* **1968**, *34*, 748. (b) Johnson, J. M.; Willits, D. A.; Young, M. J.; Zlotnick, A. Interaction with Capsid Protein Alters RNA Structure and the Pathway for In Vitro Assembly of Cowpea Chlorotic Mottle Virus. *J. Mol. Biol.* **2004**, *335*, 455.

(15) (a) Chen, C.; Daniel, M. C.; Quinkert, Z. T.; De, M.; Stein, B.; Bowman, V. D.; Chipman, P. R.; Rotello, V. M.; Kao, C. C.; Dragnea, B. Nanoparticle-Templated Assembly of Viral Protein Cages. *Nano Lett.* **2006**, *6*, 611. (b) Huang, X.; Bronstein, L. M.; Retrum, J.; Dufort, C.; Tsvetkova, I.; Aniagyei, S.; Stein, B.; Stucky, G.; McKenna, B.; Remmes, N.; Baxter, D.; Kao, C. C.; Dragnea, B. Self-Assembled Virus-Like Particles with Magnetic Cores. *Nano Lett.* **2007**, *7*, 2407. (c) Chang, C. B.; Knobler, C. M.; Gelbart, W. M.; Mason, T. G. Curvature Dependence of Viral Protein Structures on Encapsidated Nanoemulsion Droplets. *ACS Nano* **2008**, *2*, 281. (d) Daniel, M.-C.;

Tsvetkova, I. B.; Quinkert, Z. T.; Murali, A.; De, M.; Rotello, V. M.; Kao, C. C.; Dragnea, B. Role of Surface Charge Density in Nanoparticle-Templated Assembly of Bromovirus Protein Cages. *ACS Nano* **2010**, *4*, 3853. (e) Jung, B.; Rao, A. L. N.; Anvari, B. Optical Nano-Constructs Composed of Genome-Depleted Brome Mosaic Virus Doped with a Near Infrared Chromophore for Potential Biomedical Applications. *ACS Nano* **2011**, *5*, 1243.

(16) (a) Cuillel, M.; Berthetcolominas, C.; Timmins, P. A.; Zulauf, M. Reassembly of Brome Mosaic Virus from Dissociated Virus. A Neutron Scattering Study. *Eur. Biophys. J. Biophy. Lett.* **1987**, *15*, 169. (b) Chen, C.; Kao, C. C.; Dragnea, B. Self-assembly of brome mosaic virus capsids: Insights from shorter time-scale experiments. *J. Phys. Chem. A* **2008**, *112*, 9405.

(17) Zlotnick, A.; Aldrich, R.; Johnson, J. M.; Ceres, P.; Young, M. J. Mechanism of Capsid Assembly for an Icosahedral Plant Virus. *Virology* **2000**, *277*, 450.

(18) (a) Loo, L.; Guenther, R. H.; Lommel, S. A.; Franzen, S. Encapsidation of Nanoparticies by Red Clover Necrotic Mosaic Virus. *J. Am. Chem. Soc.* **2007**, *129*, 11111. (b) Aniagyei, S. E.; DuFort, C.; Kao, C. C.; Dragnea, B. Self-Assembly Approaches to Nanomaterial Encapsulation in Viral Protein Cages. *J. Mater. Chem.* **2008**, *18*, 3763. (c) Hu, Y.; Zandi, R.; Anavitarte, A.; Knobler, C. M.; Gelbart, W. M. Packaging of a Polymer by a Viral Capsid: The Interplay Between Polymer Length and Capsid Size. *Biophys. J.* **2008**, *94*, 1428.

(19) Sun, J.; DuFort, C.; Daniel, M.-C.; Murali, A.; Chen, C.; Gopinath, K.; Stein, B.; De, M.; Rotello, V. M.; Holzenburg, A.; Kao, C. C.; Dragnea, B. Core-Controlled Polymorphism in Virus-Like Particles. *Proc. Natl. Acad. Sci. U.S.A.* **2007**, *104*, 1354.

(20) Tocheva, E. I.; Li, Z.; Jensen, G. J. Electron Cryotomography. *Cold Spring Harbor Persp. Biol.* **2010**, *2*, a003442.

(21) Slot, J. W.; Geuze, H. J. A New Method of Preparing Gold Probes for Multiple-Labeling Cytochemistry. *Eur. J. Cell Biol.* **1985**, *38*, 87.

(22) (a) Chen, C.; Daniel, M.-C.; Quinkert, Z. T.; De, M.; Stein, B.; Bowman, V. D.; Chipman, P. R.; Rotello, V. M.; Kao, C. C.; Dragnea, B. Nanoparticle-Templated Assembly of Viral Protein Cages. *Nano Lett.* **2006**, *6*, 611. (b) Chen, C.; Kwak, E.-S.; Stein, B.; Kao, C. C.; Dragnea, B. Packaging of Gold Particles in Viral Capsids. *J. Nanosci. Nanotechnol.* **2005**, *5*, 2029.

(23) Mastronarde, D. N. Automated Electron Microscope Tomography Using Robust Prediction of Specimen Movements. *J. Struct. Biol.* **2005**, *152*, 36.

(24) Bohren, C. F.; Huffman, D. R. *Absorption and Scattering of Light by Small Particles*; Wiley-VCH: New York, 2008.

(25) Haynes, W. M. *CRC Handbook of Chemistry and Physics*; CRC Press: Boca Raton, FL, 2011.

(26) Schutz, C. N.; Warshel, A. What are the Dielectric "Constants" of Proteins and How to Validate Electrostatic Models? *Proteins* **2001**, *44*, 400.

(27) Gethner, J. S.; Flynn, G. W.; Berne, B. J.; Gaskin, F. Characterization of Heterogeneous Solutions Using Laser Light Scattering: Study of the Tubulin System. *Bull. Am. Phys. Soc.* **1976**, *21*, 58.

(28) Williamson, A. J.; Wilber, A. W.; Doye, J. P. K.; Louis, A. A. Templated Self-Assembly of Patchy Particles. *Soft Matter* **2011**, *7*, 3423.

(29) Zandi, R.; van der Schoot, P. Size Regulation of ss-RNA Viruses. *Biophys. J.* **2009**, *96*, 9.

(30) Novoa, R. R.; Calderita, G.; Arranz, R.; Fontana, J.; Granzow, H.; Risco, C. Virus Factories: Associations of Cell Organelles for Viral Replication and Morphogenesis. *Biol. Cell* **2005**, *97*, 147.